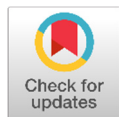


리뷰논문

## Latest Research Trends on Space Environments in Korea

Eojin Kim<sup>†</sup>, Seongsuk Lee, Bogyeong Kim

Natural Science Institute, Chungnam National University, Daejeon 34134, Korea



**Received:** October 8, 2023

**Revised:** October 24, 2023

**Accepted:** October 30, 2023

**<sup>†</sup>Corresponding author :**

Eojin Kim

Tel : +82-42-821-7492

E-mail : jinastro23@cnu.ac.kr

**Copyright** © 2023 The Korean Space Science Society. This is an Open Access article distributed under the terms of the Creative Commons Attribution Non-Commercial License (<http://creativecommons.org/licenses/by-nc/4.0>) which permits unrestricted non-commercial use, distribution, and reproduction in any medium, provided the original work is properly cited.

### ORCID

Eojin Kim

<https://orcid.org/0000-0003-4518-8468>

Seongsuk Lee

<https://orcid.org/0000-0001-9718-814X>

Bogyeong Kim

<https://orcid.org/0000-0002-4395-0407>

### Abstract

The Journal of Astronomy and Space Sciences (JASS) has published research papers on a range of topics since its initial publication in 1984, giving space science researchers a platform. In this paper, we reviewed recent publications (2019–2023) that deal with the space environment. In the space environment field, we reviewed 37 papers published in JASS during this time, covering research topics such as the sun, magnetosphere, ionosphere, atmosphere, and space radiation. We hope that researchers in the field will make use of this in the future as it will allow us to share the most recent trends in the field of space environment research that is currently underway.

**Keywords :** space environment, sun, magnetosphere, ionosphere, atmosphere, space radiation

## 1. INTRODUCTION

Since the Journal of Astronomy and Space Sciences (JASS) was first published in 1984, papers on various topics have been published as the field of space science research has steadily expanded into new areas. Jeon & Kim [1] classified all papers published from 1984, when JASS was founded, to 2018 and analyzed papers by field (see Table 1). The space-environment, space-exploration, space-application, space-technology, space-astronomy, and other categories comprised the authors' classification of all the papers published in JASS during this time frame. Within this category, the space environment was further classified as follows: sun (or solar), magnetosphere, ionosphere, atmosphere, and space radiation. Following the period examined in Jeon & Kim [1], there were 109 papers published in JASS between March 2019 and September 2023, of which 37 papers dealt with the space environment. We analyze these space environment papers recently published in JASS in order to present current research trends in the field.

The method for calculating the ionization degree of hydrogen in chromosphere [2], the statistical analysis of the solar activity cycle [3], the coronal mass ejections (CMEs) tracking model [4], and the relationship between the solar activity cycle and Earth's climate [5,6] are some of the topics of papers researching solar-related fields that will be introduced in this paper. Papers covering a wider range of magnetosphere-related subjects are available. Examining the subjects covered, these include the accuracy analysis of magnetic field models [7], observations of magnetospheric ultralow frequency (ULF) waves [8,9], modeling

**Table 1.** Subjects and details of research for classification of articles published in JASS during the period from 1984 to 2018 [1]

Subjects		Contents
1	Space environment	Sun (or solar), magnetosphere, ionosphere, space-ray
2	Space exploration	Solar system (except earth and sun), lunar exploration, space survey (including asteroids and comets)
3	Space application	Space geodesy, payload, application (including microgravity and remote sensing)
4	Space technology	Satellite operation, satellites (including space shuttles and rockets)
5	Space astronomy	Observation instruments, general astronomy, historical astronomy
6	Other	Education, meteorological (or climate)

JASS, Journal of Astronomy and Space Sciences.

of magnetosonic waves (MSW) [10,11], magnetohydrodynamic (MHD) simulation of interstellar solar wind [12], analysis of plasma sheet transition [13], observation and statistical analysis of field-aligned currents (FAC) [14,15], research trends of high-energy particles flowing into the magnetosphere [16,17], and examination of aurora observed at the Jang Bogo Station (JBS) [18].

Studies related to the ionosphere are divided into papers that study mid- to low-latitude and high-latitude regions. Topics related to the mid-to-low latitude ionosphere include effects of solar flux on equatorial electrojets (EEJ) and counter electrojets (CEJ) [19], review of ionospheric models applied to the mid-to-low latitude region [20], equatorial plasma bubbles (EPBs) observation and research trends [21,22], sporadic E or E region irregularities over the Korean peninsula [23,24], Ionospheric mid-latitude trough (IMT) [25], hemispheric asymmetry of equatorial ionization anomaly (EIA) [26], and ionospheric changes caused by earthquakes or solar eclipses [27,28] have been studied. Papers related to the polar ionosphere include polar cap and aurora observations from European Incoherent Scatter (EISCAT) radar [29] and JBS Vertical Incidence Pulsed Ionospheric Radar (VIPIR) observation results [30].

Studies pertaining to the atmosphere include thermospheric wind observation and simulation during geomagnetic storm event [31], polar mesospheric summer echoes (PMSEs) observation analysis [32], mesosphere and lower thermosphere region wind observed over Korean peninsula [33] and observations of the stratospheric and mesospheric fluctuations during stratospheric sudden warmings (SSW) [34]. Aviation radiation observation and modeling [35–37] and analysis of cosmic ray observation data using a neutron monitor [38] are the two main topics covered in published papers linked to space radiation.

## 2. METHODS

In this paper, we collected and reviewed papers published in JASS from March 2019 (Vol. 37, No. 1) to September 2023 (Vol. 40, No. 3). During this period, a total of 109 papers were published in JASS. We introduced 37 research papers corresponding to subgroups of the space environment (including sun, magnetosphere, ionosphere, atmosphere, and space radiation fields). Almost all of these papers are published in JASS as review-paper or research-paper. Papers subject to review were mainly scientific papers, and even technical papers, introducing observation equipment developed domestically included papers that performed scientific analysis on observation results. The open access JASS journal web server (<http://janss.kr>) allows you to view these works.

## 3. CLASSIFICATION BY RESEARCH TOPIC

### 3.1 Sun (Solar)

From March 2019 to September 2023, a total of 5 research papers on the sun, included in the Space Environment category, were published at JASS. A variety of topics have been studied, including the sun's chromosphere, CMEs prediction models, statistical studies of solar activity, and changes in Earth's climate due to solar activity.

The entire plasma above the minimum temperature region where hydrogen remains partially ionized, mainly made up of free electrons, protons, and hydrogen atoms, is referred to as the solar chromosphere. Because it is observable from the ground and can be used to determine the hydrogen temperature, the  $H\alpha$  line that neutral hydrogen in the chromosphere emits is useful. With the assumption of a stationary field of photoionizing radiation, Chae [2] proposed a straightforward method for calculating the degree of ionization of hydrogen using an equation corresponding to a non-LTE extension of the Saha equation. Consequently, in a chromospheric environment, a plasma feature with a temperature below 17,000K, can retain over 10% of its hydrogen in a non-ionized state, while temperatures above 23,000K result, in the majority of hydrogen being in an ionized state. Physically speaking, temperatures below 20,000K, are acceptable, given the results of the observations. It is highly likely that the temperature predicted by the  $H\alpha$  line is not real at temperatures above 25,000K because there is no neutral hydrogen present and the plasma is likely in a state of complete ionization equilibrium [2].

Chang [3] performed a statistical analysis of the linear relationship between the number of monthly sunspots and the percentage of monthly active days (AD) during the solar minimum period. The length of the solar cycle and the rising phase were also analyzed, in addition to the number of sunspots that were observed each month at solar maximum. Relationships with groups were also compared using sunspot numbers that

were newly calibrated and provided after 2015. Daily sunspot counts from the Solar Influences Data Analysis Center (SIDC), collected at various observatories worldwide during solar cycles 9 through 23 between 1843 and 2008, were the source of the data. This makes it difficult to derive the conclusion that there is a relationship between the maximum sunspot number for a given solar cycle and the slope of a linear function relating the monthly sunspot number and AD. Conversely, the length of the solar cycle was found to be, for the most part, only weakly correlated. There is debate regarding the effect of even and odd solar cycles on the slope of the monthly group number and AD linear relationship [3].

Solar explosions known as CMEs are what set off geomagnetic storms. Geomagnetic storms can result from the dynamic compression of the Earth's magnetic field by high-velocity, high-density plasma or from the recombination of the southward magnetic field component of the interplanetary CME (ICME) and the northward magnetic field component of the magnetosphere. The speed and direction of the CME can change as it travels through interplanetary space due to interactions with other CME or the solar wind. To understand changes due to the interaction of CMEs and background solar wind, Park et al. [4] developed an algorithm to track the propagation of CMEs. This algorithm uses the interplanetary scintillation (IPS) g-values recorded at a single station to predict the speed of the CMEs. With respect to a real-time CME event that happened on October 2, 2000, the developed algorithm predicted the propagation of three daily storms; the errors in arrival time and speed were 18 minutes and 20 km/s, respectively. This demonstrated that the g-values of IPS observations from the Institute for Space-Earth Environmental Research (ISEE) can be used to track the propagation of CMEs. Furthermore, statistical validation was carried out on 50 CME-ICME pair events, yielding an average error of 310 km/s for velocity and 11.14 h for arrival time [4].

Kim & Chang [5] looked into the relationships between solar variability and teleconnection indices, which affect atmospheric circulation and the spatial distribution of the global pressure system, in order to investigate the potential role of the Sun in understanding natural climate change. Using teleconnection indices [Southern Oscillation Index (SOI), Arctic Oscillation (AO), Antarctic Oscillation (AAO), and Pacific-North American (PNA)], they have computed the normalized cross-correlations of the total sunspot area, total sunspot number, and the solar north-south asymmetry. Consequently, (1) El Niño episodes most likely happen three years after a solar maximum because the SOI index has an anti-correlated relationship with both solar activity and the solar north-south asymmetry, with a lag of approximately -3 years. (2) There exists a weak or negligible correlation between solar activity and AO, AAO, and PNA index. (3) The correlations resulting from the teleconnection indices themselves are just as good as the correlations between the teleconnection and solar activity indices [5].

Chang [6] investigated relationships between the overall sunspot area and cloud properties. The total sunspot area, solar north-south asymmetry, SOI with the cloud

coverage at various altitude ranges, total column water vapor in the cloud, global surface air temperature, cloud top temperature, cloud top pressure, and cloud optical depth were all normalized cross-correlations that were determined. The following is the primary findings: (1) The extent of upper-level cloud peaks is maximum when the solar north-south asymmetry is nearly at its minimum. (2) When solar activity is decreasing, low-level clouds are at their largest. (3) Cloud coverage and the SOI index do not significantly correlate [6].

### 3.2 Magnetosphere

The papers published related to the Magnetosphere accounted for 12 of 37 papers in the entire field of Space Environment. Because the magnetosphere has so many diverse topics and the number of domestic researchers is limited, the topics of all published papers were different.

For the study of magnetospheric characteristics, it is an essential element to create a model that can well explain the magnetic field phenomenon of the magnetosphere and is similar to actual values. The Tsyganenko magnetic field model (T04, T01, T96) was examined by Song & Min [7] to determine how well it predicted changes in the geomagnetic field brought on by magnetic storms. Using Kyoto University's Dst index data from 1990 to 2016, they modeled 12 events. It was confirmed with magnetic field observation data during the event period from the Geostationary Operational Environmental Satellites (GOES), and NASA's OMNI data provided the variables required to compute the Tsyganenko magnetic field model. The simultaneous and spatial comparison was conducted between observed data and model values of the magnetic field. The T04 model, with an approximate error of 13%, would be helpful even at the location where the error is largest during geomagnetic storms. T01 performed best during quiet periods, with an average error of 8%. In addition, by identifying points with significant spatial errors during a storm, the increase in magnetotail error was quantitatively ascertained [7].

The distribution of relativistic ( $\sim 400$  keV) and ultrarelativistic ( $\sim 2$  MeV) electrons in the outer Van Allen radiation belt is highly variable. Additionally, it is recognized that a major component propelling this process are plasma waves, specifically ULF waves. The interactions between ULF wave and particle were noted by Lee et al. [8] during the geomagnetic storm's recovery phase on July 16, 2000. The global ground-based magnetometer arrays were used to collect magnetic field data. Additionally, the magnetic field and particle flux data used in this study were obtained from GOES 8 and provided by the Synchronous Orbit Particle Analyzer aboard the Los Alamos geostationary satellites. The findings demonstrate the intricate relationship between ULF waves and frequency, local time, particle energy, and particle species. Consequently, they put forth two theories to account for the flux modulation that was seen: (1) Energy-dependent

particle density gradients advecting (protons and electrons show the similar amplitude and lack of phase change with energy); (2) Energetic electronic drift resonance (distinct flux oscillations varying in amplitude and phase over various energy channels). Given the obvious connection between Pc5 waves and particle flux oscillations, Pc5 ULF waves could be crucial for electron acceleration in radiation belts [8].

In the Earth's magnetosphere, Pc1 pulsations are believed to be caused by anisotropic energetic particles ( $T_{\text{perp.}} > T_{\text{parallel}}$ ), which produce electromagnetic ion cyclotron (EMIC) waves. They are mainly generated by ring current particles with energies ranging from tens to hundreds of keV in the equatorial inner magnetosphere. Using data from the Bohyeonsan Optical Astronomy Observatory magnetic impedance (MI) ( $L = 1.3$ ), observed from November 2009 to August 2018, Kim et al. [9] examined the statistical features of Pc1 pulsation. Temporal occurrence rate variations (seasonal, diurnal, and annual) of Pc1 pulsations were studied, along with their relationship to wave properties (duration, maximum frequency, bandwidth), and geomagnetic activity indices (Kp and Dst). The following are the outcomes: (1) From late winter to early spring, PC1 waves were more common, particularly in August and after midnight (01–03 magnetic local time (MLT)). (2) Events usually lasted 2.5 minutes, with a very narrow bandwidth (within 0.1 Hz) and a maximum frequency of about 0.9 Hz. (3) During the storm, 77% of the Pc1 waves were recorded, and 90% were seen in the storm's early recovery phase [9].

MSW, or equatorial noise, are interesting because of their potential role in electron scattering in the radiation belt. Kim [10] developed an empirical model for the global distribution of these MSW. Both inside and outside the plasmasphere, MSW are usually distributed within a few degrees of magnetic latitude. The ambient plasma environment on regions experiencing MSW are the main causes of the difference between the pitch angle and the dominant energy that MSW can scatter. The Tsyganenko TS04D model and data from Electrical and Magnetic Field Instrument and Integrated Sciences mounted on a Van Allen probe were employed. According to statistics and modeling results, the intense region propagates inward toward  $L^* < 4$  and expands toward the wider MLT as Kp increases. As Kp rises in every region, the  $f_{\text{pe}}/f_{\text{ce}}$  ratio falls in distinct ways in the regions above and below  $L^* = 4$ . These results suggest that the effective scattering power of MSW depends on the geomagnetic activity and particle energy. All MLTs,  $2 \leq L^* < 6$ ,  $|\lambda| < 20^\circ$ , and  $Kp \leq 6$  are valid for the model [10].

One of the most commonly seen plasma waves in the inner magnetosphere (radial distance  $< \sim 10 R_E$ ) are near-equator MSW, which have the biggest amplitudes in the few to  $\sim 100$  Hz frequency range. In order to calculate the wave growth rate, Min & Liu [11] firstly determine the dipole magnetic field lines and the ring-shaped proton velocity distribution on the magnetic equator; secondly, they compute the linear theory dispersion relation along the field lines. The saturation amplitude was examined using a complete particle-in-cell (PIC) simulation. It is assumed here that the background and plasma magnetic fields at various points along the magnetic field lines are uniform and

treated as local. While MSW grows fastest at high latitudes ( $20^{\circ}$ – $25^{\circ}$ ), statistical observations show that the saturation amplitude actually maximizes within  $\pm 10^{\circ}$  latitude. In contrast to the observed data, the rate of decrease of the saturation amplitude was not as sharp and the average wave normal angle of the excited MSW in the simulation showed little variation with latitude. It is expected that this is due to other factors that were not considered in the current analysis, such as background magnetic field, plasma inhomogeneity, and propagation effects [11].

Understanding the nature and features of the process by which the magnetosphere receives energy, momentum, and plasma from the solar wind at the magnetosphere boundary is one of the main challenges in magnetospheric physics. Fundamental processes like pressure pulse effects, viscous-like interactions like Kelvin-Helmholtz (K-H) instability, and magnetic reconnection occur at the magnetopause boundary. Park et al. [12] performed an accurate global MHD simulation to investigate the effects of a prolonged solar wind and a weak southward interplanetary magnetic field (IMF) on the magnetic configuration and vortex structure. This leads to the following outcomes: (1) vortices are generated close to the inner site of the magnetopause following dayside reconnection; (2) the vortex propagates anti-sunward at a velocity of roughly 20–60 km/s in the dayside magnetopause region and roughly 50–150 km/s in the duskside region of the magnetopause; (3) the vortex rotates clockwise on the dawnside and counterclockwise on the duskside; (4) the magnetic field and plasma properties fluctuate quasi-periodically with a period of 8–10 min across the vortex; (5) the polar region clearly displays double twin  $\Omega_{II}$ , viscous cell, induced viscous cell, and the tail lobe convection cell and (vi) the peak value of the cross-polar cap potential varies ranging from 17 to 20 kV over a period of 8–10 min during the tail reconnection [12].

Geomagnetic activity is largely influenced by the magnetic tail region close to Earth, which lies between approximately 10 and 25  $R_E$ . In the quiet-time central plasma sheet (CPS), the average ion density and thermal energy are approximately  $0.2$ – $0.4 \text{ cm}^{-3}$  and  $2.6$ – $6 \text{ keV}$ , respectively. As magnetic activity increases, the temperature rises and the density slightly decreases. The case study of the transition boundary between the hot, rarefied plasma and the cold, dense plasma in the CPS near the midnight meridian was examined by Kim & Lee [13]. Observational data obtained from the Plasma Electron and Current Experiment, fluxgate magnetometer (FGM), and Cluster Ion Spectrometry aboard Cluster spacecraft were utilized. Furthermore, 1-minute average magnetic field and plasma data observed from OMNI/ACE were used in the analysis. Consequently, the properties of the border that divides the magnetotail into areas with distinct plasmas along the dawn-dusk direction were showcased. The plasma's characteristics suggest that plasmas from various sources may make up the near-Earth magnetotail, and it is anticipated that various dynamic processes will take place, potentially influencing the evolution of geomagnetic activity. Furthermore, it is concluded that field-aligned currents generated by the boundary layer can contribute to magnetosphere-ionosphere coupling [13].

Depending on the direction of the IMF  $B_z$ , the inner boundary of the auroral region expands (contracts) during geomagnetic storm conditions, moving toward the equator (poleward). Awuor et al. [14] defined a new metric called FAC extent in order to study latitudinal variations in storm-time mesoscale FAC. The Challenging Minisatellite Payload (CHAMP) satellite's FGM and OMNI data (Dst, IMF  $B_z$ , solar wind dynamic pressure data) from NASA/Goddard Space Flight Center (GSFC) were examined. When compared to the dawn and night sides, the analysis reveals that the equatorward shift is more pronounced on the northern dusk side at  $\sim 58^\circ$ , consistent with the minimum SymH, and  $\sim 59^\circ$  on the dayside. In the northern hemisphere dusk-dawn MLT sector, the latitudinal shift in the FAC range is more correlated with the IMF  $B_z$  than in the southern hemisphere. It is also more sensitive to dynamic pressures in the dusk-side northern hemisphere and dawn-side southern hemisphere than in the dusk-dawn zone and dawn zone of the southern hemisphere. The FAC range demonstrated a strong correlation with the dynamic pressure in the daytime (nighttime) southern hemisphere (northern hemisphere), suggesting potential electrodynamic parallels in the MLT sectors of the opposing hemisphere [14].

It is well known that the FAC surrounding the auroral region, which travels along magnetic field lines into and out of the ionosphere, is crucial to the movement of particles and energy during the solar wind-magnetosphere-ionosphere coupling process. Shin et al. [15] examined the current density seen as the Cluster constellation moved through the nightside auroral region at roughly  $4\text{--}5 R_E$  from the Earth's center in order to investigate the composition and generating mechanism of FAC. Data from February 22, 2002, when two FAC phenomena were observed in both the southern and northern hemispheres within the same current sheet for all four spacecraft, was used because the separation between the spacecraft was less than 200 km. The bipolar FAC linked to the Earthward current during the event had magnitudes of  $70.04 \text{ nA/m}^2$  at the valley and  $46.70 \text{ nA/m}^2$  at the peak, extending 516 km from valley to peak in the Southern Hemisphere. With respect to earthward currents, the mapped FAC in the northern hemisphere has a magnitude of 805 km and a magnitude of  $56.76 \text{ nA/m}^2$  [15].

Space Radiation Detector (SRD) is a part of the instruments for the study of Stable/Storm-time Space (ISSS) installed on the Next-Generation Small Satellite-1 (NEXTSat-1) that was launched in 2018. SRD consists of the High-Energy Particle Detector (HEPD), which detects electrons in the energy range of 0.35–2 MeV, and the Medium-Energy Particle Detector (MEPD) -A and -B, which detects electrons, ions, and neutral particles in the energy range of 20–400 keV. Yoo et al. [16] documented a number of SRD-related events. MEPD-A recorded an event where substorm injection led to an enhancement of the particle flux in the energy range of several tens of keV. They detected spatial distributions of electron with energies ranging from tens to hundreds of keV (MEPD) and up to few MeV (HEPD) in the slot region and outer radiation belt. They observed electron distributions over a broad energy range. It is found that the inner edge



of the outer radiation belt corresponds to the plasma transient position of L and is relatively more consistent with sub-relativistic energies than with relativistic energies [16].

It is well known that, at energies of a few 10s keV, an anisotropic distribution of energetic ions causes  $T_{\perp} > T_{\parallel}$ , thereby excitation of EMIC waves. This anisotropy can be caused by both dynamic pressure enhancement of the solar wind and substorm injection. Pitch angle scattering by EMIC waves is well known to cause relativistic electrons and energetic ions to precipitate in the atmosphere within the inner magnetosphere. Research on relativistic electron scattering and precipitation resulting from interaction with EMIC waves in the inner magnetosphere was reviewed by Lee [17]. This review addresses the advances in simulation over the last ~15 years and looks at the theory of many different issues, such as quasilinear resonant diffusion, nonlinear interactions, nonresonant interactions, the effect of a finite normal angle on pitch angle scattering, the tone emission lift, and the effects of methods of scattering pitch angle electrons near the equator [17].

Auroras, a polar upper atmosphere phenomenon also called polar light, have been observed for centuries before space research began, but the physical process has only recently begun to be understood when observation capabilities from the ground and satellites have improved due to connectivity with the ionosphere and magnetosphere. Since 2018, the JBS in Antarctica has been using the All-sky camera (v-ASC) continuously to observe aurora concurrently with the ionosphere, thermosphere, and magnetosphere (ITM). Jee et al. [18] introduced analysis procedures and observations to calculate aurora occurrence by distinguishing aurora from v-ASC image data, and provided preliminary findings regarding the aurora's temporal and spatial distribution. Based on observations, the aurora appears primarily on the northern horizon during the evening sector, stretching from the northwest to the zenith and filling nearly the whole sky over JBS at 08 MLT. In the morning sector, the aurora recedes to the northeast. At 12 MLT, auroras are distributed horizontally across the northern sky disk, showing aurora occurrences in the cusp area. This means that JBS's location is ideal for investigating aurora [18].

### 3.3 Ionosphere

The papers published related to the Ionosphere accounted for 12 of the 37 papers in the entire field of space environment. Studies mainly focus on mid- to low-latitude ionospheric phenomena.

A narrow band of strong eastward currents that flow at altitudes of 105 to 110 km above sea level within 3 degrees of latitude on either side of the equator is known as the EEJ. The westward anti-CEJ creates the H-field depression at equatorial stations when the EEJ system's flow reverses on magnetically quiet days. The F10.7 and the impact of sunspot number (R) were studied by Cherkos [19]. Ground-based magnetic data collected in 8 sections (Peru, Brazil, West and East Africa, India, Southeast Asia, Philippines, and the

Pacific) and F10.7 and R data observed from satellites during that period were used. The results show that changes in monthly average EEJ intensity are consistent with changes in solar flux and cycle of sunspot number, with strong peaks around the vernal equinox at high F10.7 and R, and strong diurnal EEJ over Peru, Southeast Asia, and the Philippines. Strong Morning-CEJ (MCEJ) observations were made over Brazil, East Africa, and Peru. During high solar cycle periods, an anti-correlation was noted between Afternoon-CEJ (ACEJ) events and F10.7 [19].

The ionized region of the upper atmosphere, known as the ionosphere, is dispersed between 60 and 1,000 km. Numerous physical processes, including chemical reactions, diffusion, wave disturbances, plasma instability, neutral winds, and transport related to electric and magnetic fields, all have an impact on the ionospheric plasma. One of the main elements of the near-Earth space environment is the ionosphere, which is closely linked to other parts of the Earth's atmosphere like the thermosphere, magnetosphere, lower atmosphere, and plasma sphere. Ionospheric predictions using observations and models are essential due to their practical impact on human society. Numerical modeling of the ionosphere is necessary not only to specify and predict space weather, but also to comprehend the physical processes that take place within the ionosphere. There are various approaches to developing ionospheric models: data assimilation modeling, theoretical modeling based on physics, and empirical modeling based on data. These three categories of ionospheric models were briefly introduced by Jee [20], who also provided an explanation of the physics-based ionospheric model using the fundamental equations governing the mid-latitude ionosphere. Additionally, boundary conditions requiring a numerical solution of the equations were discussed [20].

Aeronautics relies heavily on far-infrared wavelength observation because it provides detailed data on the temperature, composition, and particle density of the terrestrial ionosphere-thermosphere. Nevertheless, there are no known instances of climatological analysis of EPBs using Far-Ultraviolet (FUV) limb imaging devices. Park et al. [21] investigated the small-scale measurement of oxygen ion density observed in limb images of FUV on board the Ionospheric Connection Explorer (ICON) with the aim of confirming the feasibility of using EPBs in climatological analysis. Two-dimensional limb images of oxygen airglow are available in the 135.6 nm and 157 nm channels via ICON/FUV. Consequently, the ambient density shows, in agreement with earlier research, (1) the well-known zonal wavenumber-4 structures in the EIA and (2) off-equatorial enhancement above the Caribbean. As a complement to other observations from FUV disk imagers and *in-situ* plasma probes, ICON/FUV data are expected to be useful in EPBs studies [21].

It is well known that low-density plasma rising from the bottom of the F region causes the EPBs, an irregularity in electron density in the equatorial ionosphere at night. The generation mechanism and three-dimensional structure of EPBs were discussed in the review and references by Kil [39]. EPBs observed from the ground and space over the

past 100 years shows systematic seasonal and longitudinal changes and is also affected by the solar cycle. Many theories have been proposed to account for this systematic behavior of EPBs, but because it is challenging to simultaneously observe the development of causal perturbations globally, EPBs climatology remains incompletely understood. Kil [22] reviewed the climatology of EPBs occurrence confirmed through observations and the driving mechanisms currently understood [22].

Sporadic E ( $E_s$ ) is a thin layer with a thickness of roughly 1–2 km, where the electron density in the ionospheric E region at mid-latitudes is 2–3 times higher than the ambient area. It is understood to form as a result of long-term presence of metal ions from meteors that are subsequently brought together by horizontal neutral winds. Jo et al. [23] reported the  $E_s$  layer observed at the digisonde in Icheon (37.14°N, 127.54°E) and Jeju (33.4°N, 126.30°E) during the period from 2011 to 2018. At both observation sites, the incidence of  $E_s$  and the magnitude of critical frequency ( $f_oE_s$ ) peak in summer, but virtual height of the  $E_s$  layer ( $h'E_s$ ) shows semi-annual changes similar to the peak height of mesospheric meteors measured by the Sejong Science Station meteor radar (MR). Local time changes in  $h'E_s$  show semi-diurnal modulations during the equinoxes and summer months, but the changes are not evident in winter. The HWM14, IGRF12, and NRLMSISE-00 models were utilized to compute vertical ion velocities and verify their association with the semidiurnal fluctuations of  $h'E_s$  and the tidal horizontal wind [23].

Although the field-aligned irregularities (FAIs) of the ionospheric E-region have been extensively studied in the equatorial, low-latitude and auroral regions using radar and *in situ* measurements, the afternoon E-region FAI at mid-latitudes has not been previously reported. Yang et al. [24] reported the afternoon observation results of FAI in the mid-latitude E region using VHF radar. Data from a VHF coherent scattering radar (40.8 MHz frequency) that has been continuously operated in Daejeon, South Korea (36.18°N, 127.14°E) since December 29, 2009 was used. This means that: (1) afternoon E-region FAI occurrence in mid-latitudes peaks in summer and peaks in winter; (2) afternoon E-region FAI echo SNR in mid-latitudes is 35 dB, with an occurrence altitude of 100–135 km; and (3) the  $h'E_s$  observed in Icheon in the afternoon are in the height range of 105–110 km, which is approximately 5–10 km larger than the  $h'E_s$  bottom side observed at the same time. The SNR of FAI is thought to be improved by large values of  $(f_oE_s - f_bE_s)$ , indicating that patch-like  $E_s$  structures are in charge of excitation irregularities [24].

The large-scale ionospheric electron density depletion phenomenon known as the IMT happens at night in mid-latitude regions and is thought to be caused by intricate plasma processes in conjunction with the magnetosphere. In order to statistically examine the properties of the IMT, Hong et al. [25] examined upper-level sounding data from the Alouette and ISIS satellites in the 1960s and 1970s. The IMT depth rate and IMT features are stronger and more pronounced in the winter hemisphere under solar minimum conditions, even though the IMT position remains relatively constant throughout the season and solar activity. Furthermore, in the IMT region, the transition

height—where the densities of oxygen ions and hydrogen/helium ions are equal—was high at night and low during the day. St. Petersburg, situated both within and beyond the IMT region. They discovered that the electronic temperature in the IMT region is higher on winter nights, based on measurements from the Incoherent Scatter Radar (ISR) at Santin and Millstone Hill. Bipolar diffusion can propel the ionospheric plasma quickly into the magnetosphere, causing IMT depletion, when electron temperature rises [25].

The most prominent anomaly in the low-latitude ionospheric F region is the EIA, which is characterized by two enhanced plasma density peaks centered at a magnetic latitude of  $\pm 15^\circ$  off the equator. During solar minimum on the winter solstice, there is an opposite hemispheric asymmetry in the intensity of the EIA in the morning and afternoon. The interaction of the interhemispheric winds and the fountain effect, which produces EIA, explains this phenomenon. Plasma density data from CHAMP, GPS Total Electron Content (TEC) data collected between 2001 and 2008, and plasma data from the Constellation Observing System for Meteorology, Ionosphere, and Climate satellites from 2007 to 2008 were reported, according to Kwak et al. [26]. The low-latitude ionosphere's hemispheric asymmetries were examined using density data. The findings demonstrated a stronger EIA in the winter hemisphere both in the morning and afternoon during the solar maximum, and a shift in the occurrence of stronger EIA from the winter hemisphere to the summer hemisphere around 12–14 LT during the solar minimum [26].

In addition to factors such as solar and geomagnetic activity, recent studies have suggested that seismic activity can cause ionospheric changes. Using vertical TEC data from the National Oceanic and Atmospheric Administration, Park & Park [27] examined ionospheric changes brought on by seismic activity that took place in the United States between January 2013 and December 2015. The TEC fluctuations over 40 days, including the time of the earthquake, were distinguished for four regions where earthquakes of magnitude  $M \geq 5.5$  occurred, and the TEC fluctuations during earthquakes of magnitude  $5.0 \leq M < 5.5$  were examined. The findings showed that upper anomalies happened between two and eighteen days prior to the earthquake and between one and eighteen days following it. Of the twelve earthquakes with a magnitude of  $5.0 \leq M < 5.5$ , upper anomalies were found in six (50%) of the cases prior to the earthquake and in five (42%) of the cases following it. Six (75%) and five (62%) of the eight earthquakes with a magnitude of  $M \geq 5.5$  had upper anomalies prior to and following the earthquake. The TEC anomalies mentioned earlier are thought to be caused by seismic activity because the F10.7, Dst, and Kp indices show low to moderate solar and geomagnetic activity [27].

Over the past 50 years, numerous studies have examined the effects of solar eclipses on the ionosphere, making them an ideal experimental opportunity to study the effects of solar radiation on the ITM system. On August 21, 2017, between 17:20 and 18:47 UT (local daylight time), there was a total solar eclipse that crossed the United States, creating a narrow, black shadow that was roughly 160 km wide. The Swarm A and C satellites traveled 445 km during this period, entering the upper ionosphere at noon in the United

States and traveling through the lunar penumbra. Swarm mission data over the United States was used by Hussien et al. [28] to study the effects of solar eclipses on electron temperature, slanted TEC (STEC), and electron density. It can be inferred from observations that (1) a notable decrease in electron density and STEC coincided with the eclipse, possibly as a result of extreme ultraviolet reduction favoring dissociative recombination over photoionization, (2) The electron temperature in  $41^{\circ}$ – $57^{\circ}$  latitude decreased by up to 150K compared to the reference date (December 23) [28].

The northern hemisphere aurora region, which includes Kiruna, Sweden, and Sodankylä, Finland, is the subject of ionosphere studies by the international scientific association known as EISCAT, which is composed of multiple nations. This multi-site ISR system is situated in Longyearbyen, Svalbard, and Tromsø, Norway. Since 2015, the EISCAT Science Association has included the Korea Polar Research Institute (KOPRI) and the Korea Astronomy and Space Science Institute (KASI) as affiliated organizations. Jee et al. [29] analyzed observed data from December 16 – 21, 2016 and January 3 – 9, 2018, to investigate the ionospheric characteristics of the extreme/peak regions during the winter day. For this purpose, ESR observation results (electron density profile, ion drift, electron and ion temperature) were analyzed together with the High Altitude Interferometer WIND Experiment (HIWIND) provided by the National Center for Atmospheric Research (NCAR) and the High Altitude Observatory (HAO). Additionally, using long-term polar ionospheric data recorded by EISCAT radar at three sites, an investigation was carried out on the features of ion upflow generation associated with ion/electron heating in the polar ionosphere. In addition, they looked into how the polar ionospheric density profile and the mid-latitude ionosphere differ in terms of climatology [29].

Through solar wind-magnetosphere-ionosphere interaction, the polar ionosphere—where geomagnetic field lines are open—plays a significant role in the transfer of energy from the Sun to the Earth's atmosphere. Understanding the energy exchange between the magnetosphere and polar ionosphere requires constant observation, but Antarctica is much more inaccessible than the Arctic, making observations there extremely rare. A VIPIR was installed at the JBS by the KOPRI in 2015 in order to continuously monitor the ionospheric conditions in the aurora oval and polar cap region. The fundamentals of JBS-VIPIR were presented by Ham et al. [30], along with an explanation of how it can be used for Antarctic upper atmosphere research. Understanding the polar ionosphere is anticipated to be aided by the high-resolution ionospheric data (ion drift, bottom ionospheric gradient, and electron density) supplied by JBS-VIPIR in conjunction with JBS's concurrent observations of the aurora, neutral atmosphere, and magnetosphere [30].

### 3.4 Atmosphere

There are a total of 4 papers related to Earth atmosphere research, including polar atmosphere research using polar observation devices.

The magnetosphere affects atmospheric winds, which are a crucial parameter for comprehending the ionosphere, particularly during geomagnetic storms. A coupled magnetosphere-ionosphere model is needed to understand magnetospheric effects on thermospheric winds. Fabry Perot interferometry (FPI) wind observations over the mid-to-high latitudes were used by Wu et al. [31] to compare with the Multiscale Atmosphere Geospace Environment (MAGE) modeling results for the geomagnetic storm that occurred on November 3–4, 2021. The findings verified that the decline in thermosphere poleward winds at high latitudes at 22 UT on November 3 was linked to an IMF reorientation towards the north. It was also confirmed that at 10 UT on November 4, the IMF shifted to the south and poleward winds strengthened. Equatorial winds strengthened in Boulder, Colorado around midnight as the IMF turned south. Auroral events that occur simultaneously can be linked to the IMF by means of a negative component, as the wind results computed using the MAGE model clearly demonstrate [31].

Radar (frequency between 3–300 MHz) can detect PMSEs which occur at altitudes of 80–90 km (upper mesosphere and ionospheric D region). It is composed of charged ice particles of 10–50 nm in size and is known to be produced at temperatures below 150 K. Lee et al. [32] statistically analyzed wind, wave, and turbulence information provided by the ESRAD, a 52 MHz VHF mesosphere-stratosphere-troposphere radar, is situated in ESRANGE, Sweden, at 63.7°N and 21°E to estimate PMSE. In conclusion, the enhancement of PMSE was closely related to regional substorms and was especially noticeable during the 00–04 MLT period. Furthermore, the local electromagnetic field or global convective field caused by electron precipitation may have accelerated the high zonal velocities of PMSE scatterers during the substorm in the early magnetic dawn sector (00–03 MLT) [32].

The mesosphere and lower thermosphere regions are controlled by atmospheric waves of various periods. Specifically, shorter-period gravitational waves begin in the lower atmosphere, rise, and are either dissipated or broken in the upper atmosphere, altering the upper atmosphere's thermal structure and background flow. Kam et al. [33] used KASI MR observations from 2017 to 2020 to study the hourly, daily, and seasonal circulation characteristics of the east-west and south-west winds in the mesosphere and lower thermosphere region over the Korean Peninsula. The overall characteristics of the east-west and north-south winds demonstrated clear daily and seasonal variations, according to the observational data. Semi-diurnal (12-hour period) and/or diurnal (24-hour period) tides of 80–100 km were observed for both winds. When it comes to annual variation, the strongest component for both winds is annual variation, while only zonal winds exhibit semi-annual and annual variation [33].

An example of the dynamic coupling between the lower and upper atmospheres through atmospheric waves generated in the lower atmosphere and propagating upward to affect the upper atmosphere is the phenomenon known as SSW. Kim et al. [34] examined the vertical structure of temperature and ozone in the stratosphere and mesosphere during SSW by analyzing temperature and ozone observations taken by the Microwave Limb Sounder / Aura satellite between 2005 and 2016. The WACCM4 model was used to calculate the polar daily average temperature, with the results compared to that figure. Overall mesospheric temperature appeared to be uncorrelated with stratospheric temperature during the pre-phase period. The correlation was significant in the lower thermosphere and upper mesosphere during the post-phase. Ozone density was observed to vary significantly during the main- and post-phase of three SSW events. Air flowing in the polar stratosphere from mid-latitude regions during this time can be the reason for the increase in ozone density [34].

### 3.5 Space Radiation

A total of 4 studies related to space radiation were published, including papers mainly related to aviation radiation and observation results from neutron monitor.

Radiation generated at the altitude of commercial airplanes is ionizing radiation from primary protons of galactic cosmic rays and solar energetic particles. Radiation Safety Management around Living Life Act (Radiation Safety Act) stipulates annual radiation dose limits for flight attendants in Korea and the need for more accurate prediction and measurement of aviation radiation is emerging. Korea Radiation Exposure Assessment Model (KREAM), radiation prediction model is being developed to ensure radiation safety for flight crew and passengers. Hwang et al. [35] verified the KREAM model by comparing it with Liulin observations. To measure radiation exposure in aircraft, a total of 25 experiments were conducted with the Liulin-6K instrument on board commercial aircraft from March 11 to May 26 of 2020. KREAM's results were generally in very good agreement with Liulin's observations. While Civil Aviation Research Institute (CARI)-6M typically produced results that were lower than the observations, Nowcast of Atmospheric Ionizing Radiation for Aviation Safety (NAIRAS) typically produced results that were higher than the Liulin observations. Compared to the Liulin observation, KREAM showed an error of 10.95%, NAIRAS showed an error of 43.38%, and CARI-6M showed an error of 22.03%. They also found that radiation exposure can suddenly increase with altitude, especially in polar regions [35].

Since 2013, cosmic radiation exposure dose of flight crew member in Korea has been governed by the Radiation Safety Act. Members of the domestic flight crew are except from this law because they are exposed to comparatively lower route doses than members of the international flight crew. However, because of the excessively frequent flights and comparatively long total flight time, Ahn et al. [36] confirmed that the annual

cumulative dose of domestic flight crew is not negligible. Therefore, using the space radiation estimation model of the CARI-6M, NAIRAS, the annual cumulative dose of domestic flight crew was statistically analyzed in order to suggest the need for radiation exposure management of domestic flight crew. On the basis of comparison with field measurements from the KREAM and Liulin-6K LET spectrometer for NAIRAS, it was determined that the average radiation exposure dose for domestic flight crew was between 0.5 and 0.8 mSv [36].

Since the outbreak of the war in Ukraine, domestic airlines have been operating routes bypassing Russian airspace since March 15, 2022, despite longer flight times. As flight times have increased, the cosmic ray exposure dose of flight crew and passengers is expected to have also increased. Ahn et al. [37] compared the radiation exposure dose according to flight time and latitude difference before and after operating on a detour route. Latitude had little effect on the regular and detour routes for the eastern US when they operated in high latitudes above 50 degrees north latitude. Radiation exposure for the European routes was greatly impacted by the latitude difference between the normal route operating in high latitude and the bypass route operating in mid-latitude. The average reduction in radiation exposure resulting from the US East route and the European route due to the bypassing to Russia was 7.97  $\mu$ Sv and 18.73  $\mu$ Sv, respectively [37].

Muons and neutrons are common secondary particles that are produced when protons, the primary cosmic ray particle, interact with the nuclei of atmospheric gas compounds. These particles can be found underground or on the surface. It is well known that the meteorological effects of temperature cause seasonal variations in muons, and that diurnal and solar variations or transitory phenomena can cause modulations in neutron intensity over a range of time periods. By averaging daily data from the Oulu Neutron Monitor, which was in operation from January 1974 to December 2019, to the grand average and annual average, Jeong & Oh [38] reported seasonal variations in cosmic ray particles. Because of where the Earth is in its orbit, more particles enter in the early spring and early winter, and the meteorological effect of the thermal expansion causes fewer particles to enter in the summer. Additionally, because of the low cutoff, low-energy protons produce observed neutrons whereas high-energy protons produce muons [38].

## 4. SUMMARY AND DISCUSSION

Since its first publication in 1984, the JASS has published research papers on a variety of topics and has provided a research venue for researchers in the field of space science. In particular, among these areas of space science, there is a growing interest in aspects of the space environment that have an impact on real life, such as radio communications and space weather. In order to understand the latest trends in the space environment research field, this paper introduces 37 papers related to the space environment among



those recently published by JASS from 2019 to 2023. The space environment around the Earth is spatially linked starting from the sun to the magnetosphere, ionosphere, and atmosphere, and various fields are being studied, including cosmic radiation originating from the sun or outer space.

During this period, the solar chromosphere, CMEs modeling, and the connection between the solar cycle and Earth's climate were studied in the field related with Sun. Regarding the magnetosphere, various wave observations and modeling that occur within the magnetosphere have been studied, and magnetosphere modeling according to solar activity has been performed. The phenomena seen in the EIA region (asymmetry, EPB, IMT), Sporadic E, and ionospheric alterations brought on by solar eclipses or earthquakes were examined in relation to the ionosphere in the mid- and low-latitude regions. Regarding the polar ionosphere, analysis of observation results from polar observation instruments was studied. The study focused on atmospheric aspects such as atmospheric modeling, PMSEs analysis and correlation between atmospheric layers through waves. Regarding space radiation, research on aviation radiation was mainly conducted. Through this, we hope to disseminate a range of published research topics and current trends in each field and make them useful for future field researchers.

## ACKNOWLEDGEMENTS

This research was supported by the National Research Foundation of Korea (NRF-2022R1A2C1092602).

## REFERENCES

1. Jeon J, Kim Y, Analysis of papers published in the Journal of Astronomy and Space Sciences from 1984 to 2018, *J. Astron. Space Sci.* 36, 199–211 (2019). <https://doi.org/10.5140/JASS.2019.36.3.199>
2. Chae J, Ionization of hydrogen in the solar atmosphere, *J. Astron. Space Sci.* 38, 83–92 (2021). <https://doi.org/10.5140/JASS.2021.38.2.83>
3. Chang HY, Active days around solar minimum and solar cycle parameter, *J. Astron. Space Sci.* 38, 23–29 (2021). <https://doi.org/10.5140/JASS.2021.38.1.23>
4. Park SR, Jeon HC, Kim R, Kim JH, Kim SJ, et al., Development of forecast algorithm for coronal mass ejection speed and arrival time based on propagation tracking by interplanetary scintillation g-value, *J. Astron. Space Sci.* 37, 43–50 (2020). <https://doi.org/10.5140/JASS.2020.37.1.43>
5. Kim JH, Chang HY, Association between solar variability and teleconnection index, *J. Astron. Space Sci.* 36, 149–157 (2019). <https://doi.org/10.5140/JASS.2019.36.3.149>
6. Chang HY, Normalized cross-correlations of solar cycle and physical characteristics of cloud, *J. Astron. Space Sci.* 36, 225–234 (2019). <https://doi.org/10.5140/JASS.2019.36.4.225>

7. Song SM, Min K, Analysis of the Tsyganenko magnetic field model accuracy during geomagnetic storm times using the GOES data, *J. Astron. Space Sci.* 39, 159-167 (2022). <https://doi.org/10.5140/JASS.2022.39.4.159>
8. Lee E, Mann IR, Ozeke LG, Energetic electron and proton interactions with Pc5 ultra low frequency (ULF) waves during the great geomagnetic storm of 15-16 July 2000, *J. Astron. Space Sci.* 39, 145-158 (2022). <https://doi.org/10.5140/JASS.2022.39.4.145>
9. Kim J, Hwang J, Kim H, Yu Y, Statistical analysis of Pc1 pulsations observed by a BOH magnetometer, *J. Astron. Space Sci.* 37, 19-27 (2020). <https://doi.org/10.5140/JASS.2020.37.1.19>
10. Kim KC, Empirical modeling of the global distribution of magnetosonic waves with ambient plasma environment using Van Allen probes, *J. Astron. Space Sci.* 39, 11-22 (2022). <https://doi.org/10.5140/JASS.2022.39.1.11>
11. Min K, Liu K, Linear instability and saturation characteristics of magnetosonic waves along the magnetic field line, *J. Astron. Space Sci.* 37, 85-94 (2020). <https://doi.org/10.5140/JASS.2020.37.2.85>
12. Park KS, Lee DY, Kim KH, Global MHD simulation of a prolonged steady weak southward interplanetary magnetic field condition, *J. Astron. Space Sci.* 37, 77-84 (2020). <https://doi.org/10.5140/JASS.2020.37.2.77>
13. Kim HE, Lee E, Observation of transition boundary between cold, dense and hot, tenuous plasmas in the near-Earth magnetotail, *J. Astron. Space Sci.* 37, 95-104 (2020). <https://doi.org/10.5140/JASS.2020.37.2.95>
14. Awuor AO, Baki P, Olwendo J, Kotze P, Storm-time behaviour of meso-scale field-aligned currents: case study with three geomagnetic storm events, *J. Astron. Space Sci.* 36, 133-147 (2019). <https://doi.org/10.5140/JASS.2019.36.3.133>
15. Shin Y, Lee E, Lee JJ, Analysis of field-aligned currents in the high-altitude nightside auroral region: cluster observation, *J. Astron. Space Sci.* 36, 1-9 (2019). <https://doi.org/10.5140/JASS.2019.36.1.1>
16. Yoo JH, Lee DY, Kim E, Seo H, Ryu K, et al., A substorm injection event and the radiation belt structure observed by space radiation detectors onboard next generation small satellite-1 (NEXTSat-1), *J. Astron. Space Sci.* 38, 31-38 (2021). <https://doi.org/10.5140/JASS.2021.38.1.31>
17. Lee DY, Recent progress in the theoretical understanding of relativistic electron scattering and precipitation by electromagnetic ion cyclotron waves in the Earth's inner magnetosphere, *J. Astron. Space Sci.* 36, 45-60 (2019). <https://doi.org/10.5140/JASS.2019.36.2.45>
18. Jee G, Ham YB, Choi Y, Kim E, Lee C, et al., Observations of the aurora by visible all-sky camera at Jang Bogo station, Antarctica, *J. Astron. Space Sci.* 38, 203-215 (2021). <https://doi.org/10.5140/JASS.2021.38.4.203>

19. Cherkos AM, Solar flux effects on the variations of equatorial electrojet (EEJ) and counter-electrojet (CEJ) current across the different longitudinal sectors during low and high solar activity, *J. Astron. Space Sci.* 40, 45–57 (2023). <https://doi.org/10.5140/JASS.2023.40.2.45>
20. Jee G, Fundamentals of numerical modeling of the mid-latitude ionosphere, *J. Astron. Space Sci.* 40, 11–18 (2023). <https://doi.org/10.5140/JASS.2023.40.1.11>
21. Park J, Mende SB, Eastes RW, Frey HU, Climatology of equatorial plasma bubbles in ionospheric connection explorer/far-ultraviolet (ICON/FUV) limb images, *J. Astron. Space Sci.* 39, 87–98 (2022). <https://doi.org/10.5140/JASS.2022.39.3.87>
22. Kil H, The occurrence climatology of equatorial plasma bubbles: a review, *J. Astron. Space Sci.* 39, 23–33 (2022). <https://doi.org/10.5140/JASS.2022.39.2.23>
23. Jo E, Kim YH, Moon S, Kwak YS, Seasonal and local time variations of sporadic E layer over South Korea, *J. Astron. Space Sci.* 36, 61–68 (2019). <https://doi.org/10.5140/JASS.2019.36.2.61>
24. Yang TY, Kwak YS, Lee J, Park J, Choi S, The first report on the afternoon E-region plasma density irregularities in middle latitude, *J. Astron. Space Sci.* 38, 135–143 (2021). <https://doi.org/10.5140/JASS.2021.38.2.135>
25. Hong J, Kim YH, Lee YS, Characteristics of the ionospheric mid-latitude trough measured by topside sounders in 1960–70s, *J. Astron. Space Sci.* 36, 121–131 (2019). <https://doi.org/10.5140/JASS.2019.36.3.121>
26. Kwak YS, Kil H, Lee WK, Yang TY, Variation of the hemispheric asymmetry of the equatorial ionization anomaly with solar cycle, *J. Astron. Space Sci.* 36, 159–168 (2019). <https://doi.org/10.5140/JASS.2019.36.3.159>
27. Park J, Park SM, Investigation of ionospheric earthquake precursors using US-TEC data during the solar maximum of 2013–2015, *J. Astron. Space Sci.* 37, 61–68 (2020). <https://doi.org/10.5140/JASS.2020.37.1.61>
28. Hussien F, Ghamry E, Fathy A, Mahrous S, Swarm satellite observations of the 21 August 2017 solar eclipse, *J. Astron. Space Sci.* 37, 29–34 (2020). <https://doi.org/10.5140/JASS.2020.37.1.29>
29. Jee G, Ji EY, Kim E, Kwak YS, Lee C, et al., Observations for the ionosphere using European incoherent scatter (EISCAT) in the dayside polar cap/cusp and auroral region, *J. Astron. Space Sci.* 40, 1–10 (2023). <https://doi.org/10.5140/JASS.2023.40.1.1>
30. Ham YB, Jee G, Lee C, Kwon HJ, Kim JH, et al., Observations of the polar ionosphere by the vertical incidence pulsed ionospheric radar at Jang Bogo station, Antarctica, *J. Astron. Space Sci.* 37, 143–156 (2020). <https://doi.org/10.5140/JASS.2020.37.2.143>
31. Wu Q, Lin D, Wang W, Ward W, Thermospheric wind observation and simulation during the Nov 4, 2021 geomagnetic storm event, *J. Astron. Space Sci.* 39, 79–86 (2022). <https://doi.org/10.5140/JASS.2022.39.3.79>
32. Lee YS, Singh R, Jee G, Kwak YS, Kim YH, Polar mesospheric summer echo characteristics in magnetic local time and height profiles, *J. Astron. Space Sci.* 40, 101–111 (2023). <https://doi.org/10.5140/JASS.2023.40.3.101>

33. Kam H, Kwak YS, Yang TY, Kim YH, Kim J, et al., Characteristics of horizontal winds in the mesosphere and lower thermosphere region over Korean peninsula observed from the Korea astronomy and space science institute meteor radar, *J. Astron. Space Sci.* 38, 229-236 (2021). <https://doi.org/10.5140/JASS.2021.38.4.229>
34. Kim JH, Jee G, Choi H, Kim BM, Kim SJ, Vertical structures of temperature and ozone changes in the stratosphere and mesosphere during stratospheric sudden warmings, *J. Astron. Space Sci.* 37, 69-75 (2020). <https://doi.org/10.5140/JASS.2020.37.1.69>
35. Hwang J, Kwak J, Jo G, Nam U, Validation of KREAM based on in-situ measurements of aviation radiation in commercial flights, *J. Astron. Space Sci.* 37, 229-236 (2020). <https://doi.org/10.5140/JASS.2020.37.4.229>
36. Ahn HB, Hwang J, Kwak J, Kim K, Analysis of cosmic radiation exposure for domestic flight crews in Korea, *J. Astron. Space Sci.* 39, 51-57 (2022). <https://doi.org/10.5140/JASS.2022.39.2.51>
37. Ahn HB, Kwak J, Hwang J, Comparative analysis of cosmic radiation exposure dose due to the Russian detour route, *J. Astron. Space Sci.* 40, 59-66 (2023). <https://doi.org/10.5140/JASS.2023.40.2.59>
38. Jeong J, Oh S, Seasonal variation of cosmic ray intensity observed by the Oulu neutron monitor, *J. Astron. Space Sci.* 37, 165-170 (2020). <https://doi.org/10.5140/JASS.2020.37.3.165>
39. Kil H, The morphology of equatorial plasma bubbles: a review, *J. Astron. Space Sci.* 32, 13-19 (2015). <https://doi.org/10.5140/JASS.2015.32.1.13>

## Author Information

**Eojin Kim** jinastro23@cnu.ac.kr



She studied the ionosphere using satellite and ionosonde data at the Department of Astronomy and Space Science at Chungnam National University, and earned a doctorate in ionospheric prediction modeling over the Korean Peninsula. Since then she has worked at KARI, SaTReC, KISTEP, and is currently a postdoctoral researcher at the Natural Science Research Institute of Chungnam National University, where she conducts lunar and planetary environment research.

**Bokyeong Kim** bkastro@cnu.ac.kr



She received her doctorate in 2020 from the Department of Space Geology at Chungnam National University, and has been working as a postdoctoral researcher at the Natural Science Research Institute of Chungnam National University since 2021. Currently she is conducting solar dynamo research.

**Seongsuk Lee** ssllee20@cnu.ac.kr



She conducted research on high-energy charged particles incident on Earth using spacecraft neutron detector data at the Department of Astronomy and Space Science at Chungnam National University. At the Department of Space Geology at the same university, she conducted research on the geological link between deep-sea temperatures in the Pacific Ocean using satellite and reanalysis field data. She is currently a full-time researcher at the Natural Science Research Institute of Chungnam National University, where she conducts global climate change research utilizing large-capacity ocean satellite observations.